Journal Pre-proof

Pd and Octahedra Do Not Get Along: Square Planar [PdS_4] Units in Non-Centrosymmetric $La_6PdSi_2S_{14}$

Georgiy Akopov, Gayatri Viswanathan, Nethmi W. Hewage, Philip Yox, Kui Wu, Kirill Kovnir

PII: S0925-8388(22)00147-5

DOI: https://doi.org/10.1016/j.jallcom.2022.163756

Reference: JALCOM163756

To appear in: *Journal of Alloys and Compounds*

Received date: 10 December 2021
Revised date: 7 January 2022
Accepted date: 10 January 2022

Please cite this article as: Georgiy Akopov, Gayatri Viswanathan, Nethmi W. Hewage, Philip Yox, Kui Wu and Kirill Kovnir, Pd and Octahedra Do Not Get Along: Square Planar [PdS_4] Units in Non-Centrosymmetric $La_6PdSi_2S_{14}$, *Journal of Alloys and Compounds,* (2021) doi:https://doi.org/10.1016/j.jallcom.2022.163756

This is a PDF file of an article that has undergone enhancements after acceptance, such as the addition of a cover page and metadata, and formatting for readability, but it is not yet the definitive version of record. This version will undergo additional copyediting, typesetting and review before it is published in its final form, but we are providing this version to give early visibility of the article. Please note that, during the production process, errors may be discovered which could affect the content, and all legal disclaimers that apply to the journal pertain.

© 2021 Published by Elsevier.

Pd and Octahedra Do Not Get Along: Square Planar [PdS_4] Units in Non-Centrosymmetric $La_6PdSi_2S_{14}$

Georgiy Akopov[1,2], Gayatri Viswanathan[1,2], Nethmi W. Hewage[1,2], Philip Yox[1,2], Kui Wu[3], Kirill Kovnir[1,2,*]

[1]*Ames Laboratory, U.S. Department of Energy, Ames, IA 50011, United States.*

[2]*Department of Chemistry, Iowa State University, Ames, IA 50011, United States.*

[3]*Hebei University, Baoding City, Hebei Province, 830011, China.*

*Corresponding authors: kovnir@iastate.edu

Journal Pre-proof

ABSTRACT

Non-linear optical (NLO) materials require a balance of high second-harmonic generation (SHG) signal and laser damage threshold (LDT), as well as phase matchable behavior. Herein, we report a new member of the $(RE)_6(TM)_x(Tt)_2Q_{14}$ family of compounds, $La_6PdSi_2S_{14}$, which, unlike all other reported *TM* analogues crystallizing in hexagonal $P6_3$ space group, crystallizes in the non-centrosymmetric monoclinic $P2_1$ space group. The crystal structure contains chains of edge-sharing distorted square planar [PdS_4] units. The square-planar coordination of Pd in $La_6PdSi_2S_{14}$ exhibits remarkable NLO properties with high SHG (3.7 × $AgGaS_2$) and LDT (3 × $AgGaS_2$) values as well as phase matchability. This shows the promise of novel materials with distorted structural motifs for enhanced NLO properties. Upon formation of bimetallic chiral sulfides containing both Cu and Pd, Cu occupies the opposite faces of the octahedra forming [CuS_3] units while Pd can be stabilized in the center of PdS_6 octahedra in the hexagonal $P6_3$ crystal structure of $La_6Pd_{0.5}CuSi_2S_{14}$. This suggests that it is possible to form mixed metal systems which could further enhance NLO properties by incorporation of additional structural distortions.

keywords: Chiral; polar: square-planar;crystal structure: non-linear optical properties

Journal Pre-proof

INTRODUCTION

Many applications in fields such as atmospheric sensing, medicine, imaging (materials and biology), and telecommunications require novel laser materials which, in turn, drives the need for research in new non-linear optical (NLO) materials.[1,2] In order to generate a second-order non-linear response, the material in question has to possess a non-centrosymmetric crystal structure with a certain crystal packing pattern and alignment of the structural units (tetrahedra, octahedra, etc.) in the structure.[3–10] A good balance of second-harmonic generation (SHG) and laser-damage threshold (LDT), as well as phase-matchability, are required.

$(RE)_6(TM)_xZ_2Q_{14}$ (*RE* = rare-earth; *TM* = transition metals; Z = tetrels (Si, Ge and Sn), triels (B, Al, Ga, and In) as well as some group II (Be), transition metals (Fe, Zn), and lanthanides (Sm and Yb); *Q* = S and Se) is a large class of compounds which crystallizes in the chiral, polar, and non-centrosymmetric $P6_3$ space group.[11,12] For simplicity, we will use *Tt* notation to describe compositions with Si and Ge. For $(RE)_6(TM)_x(Tt)_2Q_{14}$ $x = 2/n$, where *n* is the oxidation state of the metal (TM^{n+} = Cu^+, Li^+, Mn^{2+}, Rh^{3+}, Hf^{4+}, etc.).[12] While these phases possess non-linear optical properties due to the non-centrosymmetric space group, the reason for the different values of SHG and LDT values of its members is not entirely understood. Among phases with trigonal planar *TM*-S geometry ($[(TM)S_3]$), $La_6Cu_2Ge_2S_{14}$ showed a good balance of SHG and LDT and phase matchability, while $La_6Cu_2Si_2S_{14}$ showed poor SHG response.[12] For structures with octahedral $[(TM)S_6]$ units, SHG activity depends on the concentration, oxidation state, and spin state of the transition metal; for example, structures with low spin d^6 Rh^{3+} (1/3 octahedra occupied) show better activity than those with Co^{2+} located in ½ of all octahedra.[12] The compositions where all octahedra are occupied (i.e. Li^+) have shown good SHG and LDT values.[13] As a result, structure-property relationships for non-linear optical behavior is approached as a weighted combination of multiple parameters:

overall crystal structure, packing of structural motifs, nature of the constituent elements, and crystallographic disorder.

Recently, defective and distorted diamond-like structures have shown promise as candidates for non-linear optical properties with good SHG and LDT for $Hg_3P_2S_8$.[14,15] In this structure, mercury forms two types of [HgS_4] tetrahedra with one being highly distorted. The high SHG response in the material is attributed to synergy of the highly distorted [HgS_4] and ordered [PS_4] units, as well as vacancy-induced non-bonding electrons. The case for structural units with Hg^{2+} (d^{10} configuration) as well as d^5 (Mn^{2+}) and d^0 (Sc^{3+}, Zr^{4+}) have shown to be favorable in producing strong SHG signals in NLO materials.[16–18]

Here, we report a quaternary sulfide $La_6PdSi_2S_{14}$, which represents a new *TM*-S structural unit in the $(RE)_6(TM)_x(Tt)_2Q_{14}$ class of materials: edge-sharing distorted square planar [PdS_4] units. Unlike materials with Pd group members (Ni and Pt) which crystallize in the hexagonal $P6_3$ space group ($La_6NiSi_2S_{14}$ and $La_6Pt_{0.5}Si_2S_{14}$), the Pd analogue adopts the non-centrosymmetric monoclinic $P2_1$ space group. The [PdS_4] units are derived from octahedra where the axial bonds become significantly elongated and the local coordination of Pd distorts into square planar geometry. It was further found that upon incorporation of a heavier tetrel (Ge), the overall crystal structure remains $P2_1$ but the degree of distortion of the unit cell from the hexagonal archetype is smaller than in the Si case. As a result, $La_6PdGe_2S_{14}$ features highly distorted [PdS_6] octahedral units. It is also possible to stabilize Pd-Si structure in the hexagonal form by partially substituting Pd with Cu forming $La_6Pd_{0.5}CuSi_2S_{14}$. In this case, Pd occupies the positions at the center of the octahedra as [PdS_6] and Cu occupies the opposite faces of the octahedra as [CuS_3]. $La_6PdSi_2S_{14}$ has shown a good combination of SHG (3.7× $AgGaS_2$) and LDT (3× $AgGaS_2$), as well as phase-matchability, showing that structural disorder and distortions can promote an enhancement in non-linear optical properties.

EXPERIMENTAL METHODS

Synthesis

Materials used: S powder (99.5%, Alfa Aesar, USA), potassium iodide (KI) salt (99%+, Strem, USA). La pieces as well as Pd, Si, and Ge were acquired from the Materials Preparation Center at Ames Laboratory, which is supported by the US DOE Basic Energy Sciences: La chunk (99.9999%), Cu pellets (99.995%), Pd rod (99.99%), Si lumps (99.9999996%), and Ge lumps (99.999%).

Precursors: *RE-TM-Tt* precursors were prepared using pieces of appropriate metals and tetrels. Samples with a total mass of 0.6 - 1 g were weighed out in a ratio of *La*:*TM*:*Tt* = 6:*x*:2.05 (*Tt* = Si and Ge; *TM* = Cu, Pd; *x* = 1 for Pd; and *x* = 2 for Cu). Details of arc-melting procedure can be found elsewhere.[12,19–22]

Single crystals were grown using pre-arc-melted precursor, S powder, and potassium iodide (KI) salt flux. The ratio of (precursor + S) to KI flux was kept at 1 to 30 ratio by mass (e.g. for 0.1g of reactants, 3g of KI was used). The reactants and KI salt were added to a silica ampule, which was sealed under vacuum. The reaction products were washed with deionized water to remove KI flux, the sample was then vacuum filtered and allowed to dry.

Bulk powders of the materials were synthesized using the appropriate pre-arc melted precursor (or a pair of precursors for Pd/Cu solid solutions ($Pd_{1-y}Cu_{2y}$), where y = 0.1 to 0.9) and sulfur powder. Samples were prepared by loading the silicide binary and sulfur (1:14 ratio) in a fused silica ampoule, which were then flame sealed under vacuum.

For both crystals and bulk powders, the samples were heated over 12 hours to 1000 – 1050^{o}C, dwelled for 72 - 120 hours and then cooled to room temperature over 8 hours.

X-ray Diffraction

Powder X-ray diffraction (PXRD) was performed using a Rigaku Miniflex 600 with Cu-K_α radiation and a Ni-K_β filter. Sample holders were composed of zero-background silicon plates.

Single crystal X-ray diffraction (SCXRD) was performed using a Bruker D8 Venture diffractometer using Mo-K_α radiation. All crystal datasets were collected at 100 K under a N_2 stream. All datasets had ω-scans recorded at a 0.3 - 0.6° step width and were integrated with the Bruker SAINT software package. Structure determination and refinement of the crystal structures were carried out using the SHELX suite of programs.[23] The site occupancies of transition metals (Pd or Cu) were refined in all cases. In the crystal structures of $La_6PdSi_2S_{14}$ and $La_6CuPd_{0.5}Si_2S_{14}$, the sulfur atoms surrounding Pd were split into two sites with partial occupancies. The crystals of $La_6PdGe_2S_{14}$ were of low quality and heavily twinned. The reported crystal structure was produced from a 6-component twin with many La, Pd, and S disordered atomic sites. In the structure of $La_6PdGe_2S_{14}$, all atoms were refined isotropically.

Scanning Electron Microscopy/Energy Dispersive Spectroscopy (SEM/EDS)

Elemental analysis of samples was conducted using a FEI Quanta 250 field emission-SEM with EDS detector (Oxford X-Max 80, ThermoFischer Scientific, Inc., USA) and analyzed using the Aztec software. Powder samples were mounted in epoxy, polished to a level surface, and coated with a conductive layer of carbon. Large crystals were mounted on double-sided carbon tape. An accelerating voltage of 15kV was used to study all samples.

DFT Calculations

Journal Pre-proof

Electronic structure calculations were performed using the Vienna Ab intio Simulation Package (VASP), which uses a plane-wave basis set with projector-augmented-wave (PAW) potentials.[24–26] Perdew-Burke-Ernzerhof (PBE) generalized gradient functionals were used to study monoclinic and hexagonal variants of $La_6TMSi_2S_{14}$ (*TM* = Ni, Pd).[26–28] A 1×1×2 supercell was used to simulate alternating *TM*-filled and empty polyhedra in both structure types. An energy cutoff of 500 eV was applied. The linear tetrahedron method was used for integrating the irreducible wedge of the Brillouin zone with a *Γ*-centered *k*-point grid of 10×10×10.[29,30] Electronic and structure optimization criteria were set to 1×10^{-4} eV and -0.02 eV, respectively.

Solid-State Diffuse Reflectance Spectroscopy

The UV/Vis diffuse reflectance spectra were measured from 200-1080 nm with a BLACK-Comet C-SR-100 spectrometer. Powder samples were finely ground and flattened on a microscope slide. Band gaps were estimated through extrapolation of the linear slope in the corresponding Tauc plots by plotting $(A\textit{hv})^{1/r}$ vs *hv* where r = ½ for direct and r = 2 for indirect band gaps.

Second Harmonic Generation (SHG) and Laser Damage Threshold (LDT)

Through the Kurtz and Perry method, powder SHG responses were investigated by a Q-switch laser (2.09 μm, 3 Hz, 50 ns) with different particle sizes, including 38−55, 55−88, 88−105, 105−150, 150−200, and 200−250 μm. Due to the narrow bandgaps of title compounds, the SHG response may be seriously underestimated by detecting transmittance SHG intensity signals. Thus, in this work, we chose the more feasible measurement method through collecting the special reflectance SHG intensity signals on the sample surface instead of common transmittance signals, and this method was confirmed elsewhere to be credible.[31,32]

The $AgGaS_2$ crystal was ground and sieved into the same size range as the reference. The LDTs were evaluated on the powdered sample (38-55 μm) with a 1.06 μm pulsed YAG laser. Similar size of $AgGaS_2$ was chosen as the reference. To adjust different laser beams, an optical concave lens is added into the laser path. The damage spot is measured by the scale of an optical microscope.

RESULTS AND DISCUSSION

While most members of the $(RE)_6(TM)(Tt)_2Q_{14}$ family of compounds crystallize in the hexagonal $P6_3$ space group[12,33,34], compositions with Pd belong to the non-centrosymmetric monoclinic $P2_1$ space group (**Table 1 and Figure 1**). $P2_1$ is a maximal non-isomorphic subgroup of $P6_3$, they are related by *t*3 *translationgleich* transformation. The structure of $La_6PdSi_2S_{14}$ consists of spiral columns of face-sharing $[LaS_7]$ prisms which are wound around a chain of edge-sharing distorted pseudo-square planar $[PdS_4]$ units with $[SiS_4]$ tetrahedral units surrounding the $[LaS_7]$ column. Since the charge on Pd is 2+, the Pd site is half occupied meaning only half of $[TMS_4]$ squares contain the Pd metal in the center.

In the $[PdS_4]$ square planar units, the interior quadrilateral S-Pd-S angles are slightly smaller or larger than 90^o (**Table 2 and Figure 2**). The Pd-S bond lengths of the "filled" units are 2.39-2.43 Å, comparable to Pd-S bonds in other square planar compounds (**Table 3**). Square planar local coordination of Pd by S is common and found in many reported binary and multinary Pd sulfides. The $[PdS_4]$ unit can be "extended" to form a full pseudo-octahedron by including the long axial Pd1-S3 bonds of 3.03 Å (**Figures 1 and 2**). The volumes for the empty and filled pseudo-octahedra are 23.49 (comparable to the volumes of other $[TMS_6]$ octahedra) and 27.11 $Å^3$ (slightly smaller than the empty octahedra for other *TM*), respectively.[12]

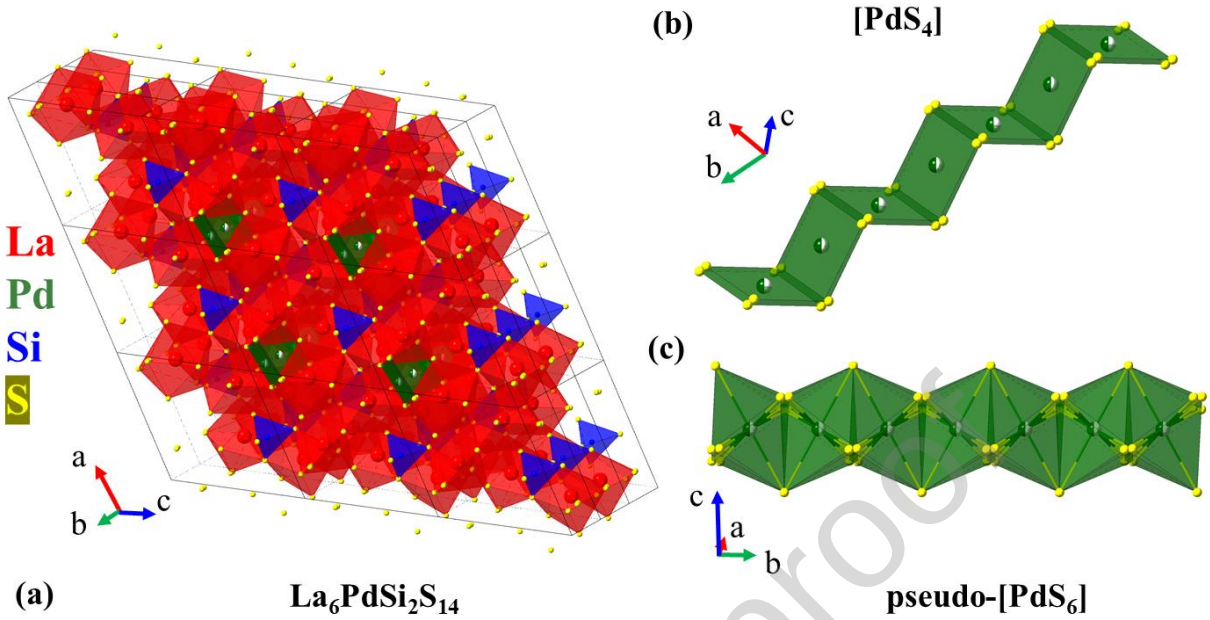

Figure 1. (a) Crystal structure of $La_6PdSi_2S_{14}$: [LaS_7] polyhedra (red), [SiS_4] tetrahedra (blue), [PdS_4] square planar units (green). (b) Chain of edge-sharing [PdS_4] units; (c) Chain of face-sharing pseudo-[PdS_6] octahedral units. Pd-S bonds in square plane are 2.390-2.434 Å, while the longer axial bonds used to construct pseudo-octahedra are 3.031-3.033 Å.

Table 1. Crystal structure parameters and EDS composition for multinary phases.[a)]

Refined composition	$\mathbf{La_6Pd_{0.96(2)}Si_2S_{14}}$	$\mathbf{La_6Pd_{0.93(2)}Ge_2S_{14}}$	$\mathbf{La_6Pd_{0.51(2)}Cu_{0.91(3)}Si_2S_{14}}$
Composition from EDS	$La_6Pd_{0.99(4)}Si_{1.98(4)}S_{13.1(1)}$	$La_6Pd_{0.88(4)}Ge_{2.0(1)}S_{13.2(1)}$	$La_6Pd_{0.63(3)}Cu_{0.79(6)}Si_{2.69(16)}S_{12.6(2)}$
CSD-number	2126977	2126975	2126976
Space group	$P2_1$	$P2_1$	$P6_3$
λ (Å)	Mo-K_α: 0.71073		

T (K)	100(2)	173(2)	173(2)
a (Å)	10.0053(9)	10.226(2)	10.2973(4)
b (Å)	5.7576(6)	5.8377(12)	10.2973(4)
c (Å)	10.3351(10)	10.320(2)	5.7878(3)
β (°)	117.932(3)	119.495(6)	120
V (Å^{-3})	526.01(9)	536.2(2)	531.48(5)
Z	1	1	1
ρ (g•cm^{-3})	4.548	4.731	4.537
Abs. corr.	multi-scan		
μ (mm^{-1})	14.19	16.54	14.58
θ (°)	2.23 – 40.22	2.27 – 35.30	2.28 – 39.92
Data / param.	3954 / 116	1833 / 75	1798 / 49
R_1	0.032	0.064	0.036
wR_2	0.057	0.148	0.070
Goodn.-of-fit	1.02	1.08	1.10
Flack Param.	0.02(3)	Refined as a 6-component twin	0.04(2)
Diff. peak/hole (e$^-$ •Å^{-3})	1.96 / -1.96	3.14 / -2.65	1.75 / -1.77

[a)] Further details of the crystal structure investigations may be obtained from the joint CCDC/FIZ Karlsruhe online deposition service: https://www.ccdc.cam.ac.uk/structures/? by quoting the CSD deposition numbers: 2126975-2126977.

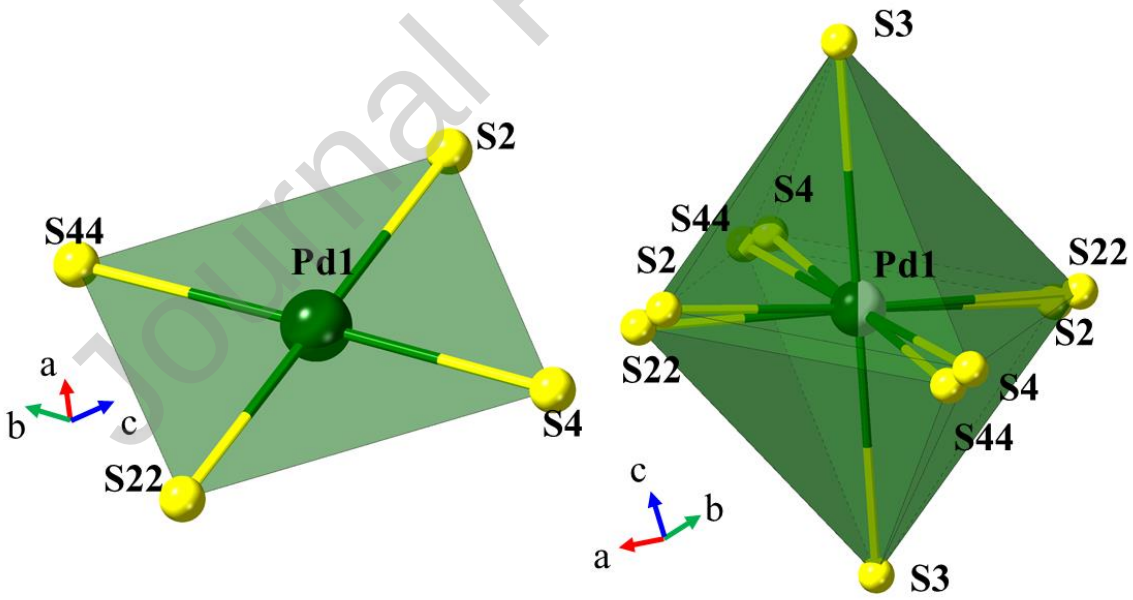

Figure 2. Structural units in $La_6PdSi_2S_{14}$: (**left**) Square planar [PdS_4] unit; (**right**) pseudo-octahedral [PdS_6] unit.

Table 2. Pd-S bond length and S-Pd-S bond angles in the square planar [PdS_4] and pseudo-octahedral [PdS_6] units of $La_6PdSi_2S_{14}$.

Bond Length (Å)	**Filled □**	**Empty □**	**Bond Angles (°)**	**Filled □**	**Empty □**
Pd-S2	2.389	2.615	S2-Pd-S4	91.647	82.420
Pd-S4	2.399	2.598	S2-Pd-S44	89.049	97.871
Pd-S22	2.433	2.611	S22-Pd-S44	91.583	83.511

Pd-S44	2.417	2.602	S4-Pd-S22	87.731	96.041
Pd-S3	3.031 – 3.033	-	S4-Pd-S44	179.141	179.110
			S2-Pd-S22	178.690	178.460

$La_6PdGe_2S_{14}$ crystals obtained from KI flux were heavily twinned and the best solution was refined as a six-component twin (**Table 1**). Upon substituting Si with a larger tetrel, Ge, the structure remains monoclinic $P2_1$ but is less distorted from the hexagonal archetype. Lattice parameters *a* and *c* are more similar in the Ge analogue compared to the Si case (~0.1 Å (0.9%) difference *vs.* ~0.3 Å (3.2%)), and the β angle is almost 120° (**Table 1**). In this structure, Pd is split between two positions: Pd1 (39% occupancy) is at the center of a distorted octahedron and Pd11 (8% occupancy) is off the trigonal plane located at the opposite faces of the octahedron. In both cases Pd atoms remain in 2+ oxidation state, meaning half of octahedra are occupied. The Pd distribution over these two sites is similar to $Y_6PdSi_2S_{14}$, where Pd is split between the octahedral and trigonal planar positions.[34] Furthermore, such cases with split metal positions (octahedral and trigonal planar) have been reported for $Ln_6Ag_xSi_2S_{14}$ (Ln = La - Sm).[35] In $La_6PdGe_2S_{14}$, Pd-S bonds for the "filled" octahedra are 2.418 – 2.772Å, with the volume being 21.69 $Å^3$ (**Figure 3 left** and **Table 4**). The presence of "empty" and "filled" octahedra leads to split S positions (S5/S55, S6/S66 and S7/S77) between the [PdS_6] octahedra and [LaS_7] polyhedra.

Table 3. Pd-S bond lengths for select compounds with different Pd-centered structural motifs.

Phase	**d(Pd-S) (Å)**	**Reference**	**Phase**	**d(Pd-S) (Å)**	**Reference**
Square-planar			*Octahedral*		
PdS	2.340 – 2.346	[36]	Co_8PdS_8	2.502	[37]
$BaPdS_2$	2.465	[38]	$(Fe_4Ni_4)PdS_8$	2.554	[37]
$Cs_2Pd_3S_4$	2.317 – 2.356	[39]	$Pd_2(P_2S_6)$	2.548 – 2.555	[40]
Na_2PdS_2	2.351 – 2.385	[41]	$Y_6PdSi_2S_{14}$	2.576 – 2.558	[34]
$CePd_3S_4$	2.373	[42]	*Tetrahedral*		
$Pd_3(PS_4)_2$	2.342	[43]	PdU_2S_4	2.377 - 2.594	[44]
Nb_2PdS_6	2.324	[45]			
$KPd(PS_4)$	2.323-2.334	[46]			

Since Ni^{2+} can form $La_6NiSi_2S_{14}$ with Ni located in the center of almost regular S_6 octahedra,[11] we investigated whether it is possible to form a Pd-containing hexagonal

structure. This was achieved through partial substitution of Pd with Cu. Addition of copper results in the formation of $La_6Pd_{0.5}CuSi_2S_{14}$, which crystallizes in the hexagonal $P6_3$ space group. In this structure Pd^{2+} occupies the positions in the center of the octahedra, while Cu^+ occupies the trigonal planar positions at the opposite faces on the octahedra (**Figure 3 right**). The presence of "empty" and "filled" octahedra again leads to split S positions (S3 and S33). As a result, Pd-S bond lengths in the "filled" octahedra are 2.445 – 2.585 Å, while the "empty" octahedra are elongated with 2.695 – 2.733 Å distances from S to the center. On the other hand, the Cu-S bonds are 2.299 Å, comparable to the Cu-S bonds in $La_6Cu_2Si_2S_{14}$ at 2.276 Å (**Table 4**). Cu^+ sits in the trigonal faces of the elongated "empty" (no Pd^{2+}) octahedra, while Pd^{2+} sits in the "filled" contracted octahedra. **Table 5** provides a comparative summary of bond lengths and polyhedral volumes between the three novel crystal structures and previously reported $La_6Cu_2Si_2S_{14}$.

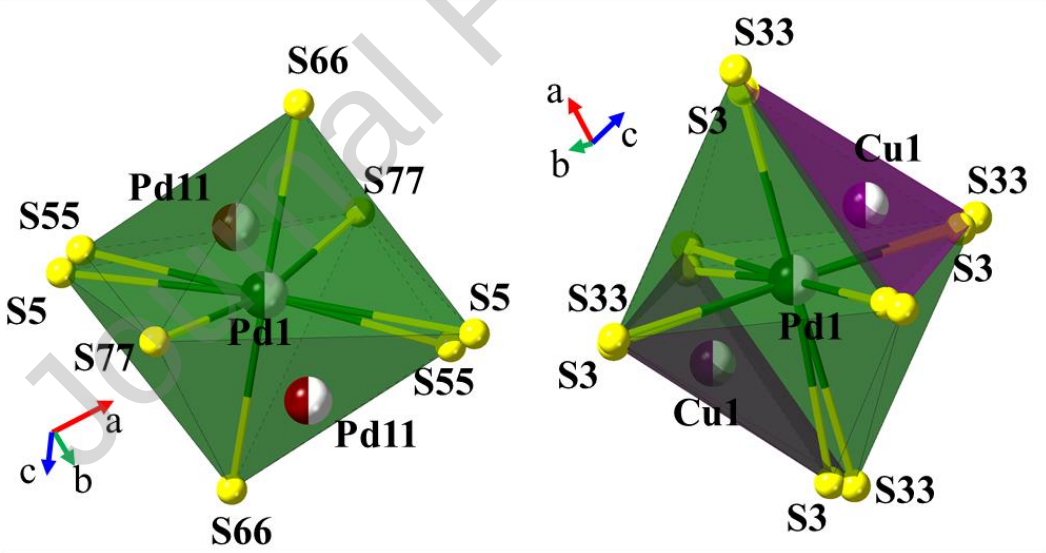

Figure 3. Distorted octahedral [PdS_6] and distorted trigonal planar [(*TM*)S_3] units for: (**left**) $La_6PdGe_2S_{14}$; and (**right**) $La_6Pd_{0.5}CuSi_2S_{14}$.

Table 4. *TM*-S bond length and S-*TM*-S bond angles (*TM* = Pd and Cu) in the distorted trigonal planar [(*TM*)S_3] and distorted octahedral [PdS_6] units of $La_6PdGe_2S_{14}$ and $La_6Pd_{0.5}CuSi_2S_{14}$.

$La_6PdGe_2S_{14}$		**$La_6Pd_{0.5}CuSi_2S_{14}$**	
Bond Length	**d (Å)**	**Bond Length**	**d (Å)**
[PdS_3]		[CuS_3]	
Pd11-S5	2.343	Cu1-S33	2.299

Pd11-S77	2.296		
Pd11-S66	2.081		
[PdS_6]		[PdS_6]	
Pd1-S55	2.485 – 2.559	Pd-S3	2.445 – 2.585
Pd1-S66	2.552 – 2.592		
Pd1-S77	2.417 - 2.772		
Bond Angles	**σ (°)**	**Bond Angles**	**σ (°)**
S66-Pd1-S66 (across Pd1)	178.715	S3-Pd1-S3 (across Pd1)	175.468
S77-Pd1-S77 (across Pd1)	168.443		
S55-Pd1-S55 (across Pd1)	177.620		
S66-Pd1-S77	72.016 – 77.404	S3-Pd1-S3	89.703
S66-Pd1-S55	86.004 – 88.441		
S55-Pd-S77	68.179 – 80.873		

Table 5. Comparison of Pd-S and Cu-S interatomic distances and volumes of octahedra in $La_6(TM)(Tt)_2S_{14}$ (*TM* = Pd, Cu; *Tt* = Si, Ge).

Phase $La_6(TM)(Tt)_2S_{14}$	**Filled Octahedra**		
	d(Pd-S)$_{Oh}$ (Å)	**d(*TM*-S)$_{\Delta}$ (Å)**	**V$_{oh}$ (Å^3)**
Cu - Si[12]	-	2.276	-
Pd/Cu - Si	2.445 – 2.585	2.299	21.17
Pd - Si	2.289 – 2.433 (3.033)[a]	-	23.49
Pd - Ge	2.417 – 2.778	2.081 – 2.343	21.69

[a]Pd-S bond to the axial S3 sulfur used to construct the pseudo-octahedron.

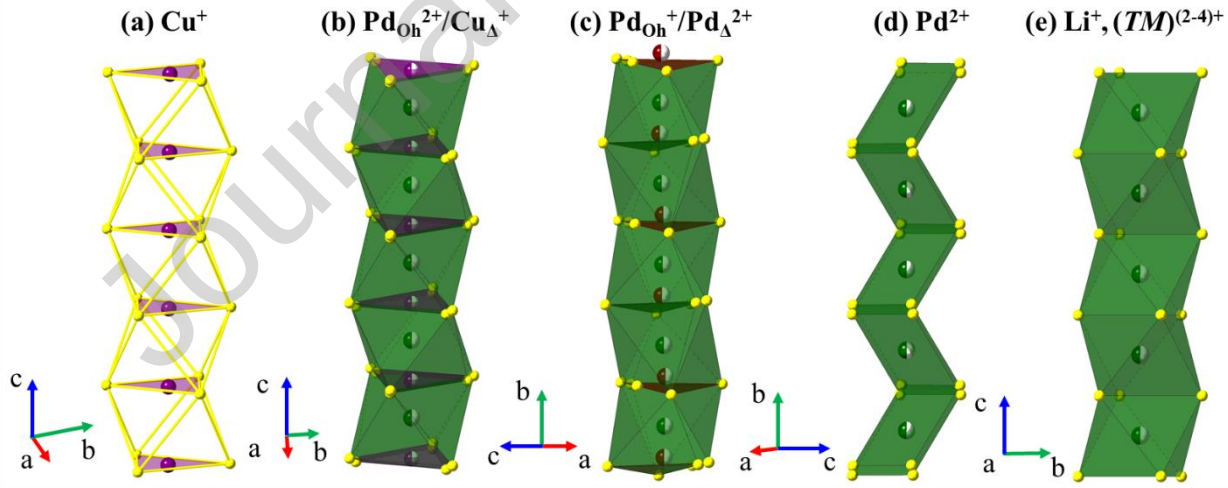

Figure 4. *TM*-centered structural units observed in the chains of $La_6(TM)_x(Tt)_2S_{14}$: (a) trigonal planar [(TM)S_3] units located on the faces of the octahedra for *TM* = Cu, Ag, and Au; (b) trigonal planar [CuS_3] and octahedral [PdS_6] units in the structure of $La_6Pd_{0.51}Cu_{0.91}Si_2S_{14}$; (c) trigonal planar [$PdS_3$] and octahedral [$PdS_6$] units in the structure of $La_6PdGe_2S_{14}$; (d) edge-sharing square planar [PdS_4] units in the structure of $La_6PdSi_2S_{14}$; (e) face-sharing octahedral [(*TM*)S_6] units observed for Li and most *TM*'s.

Journal Pre-proof

Considering all the possible variations of [(*TM*)S_6] geometries, it is possible to construct a representative structural series (**Figure 4**). For known 1+ transition metals (Cu, Ag and Au), the trigonal planar [(*TM*)S_3] metal-sulfur fragments compose the opposite faces of face-sharing octahedra (**Figure 4a**). Face-sharing metal-centered [(*TM*)S_6] octahedron is another type of common structural unit for other 2+, 3+ and 4+ transition metals (except Pd^{2+}) and Li^+ (**Figure 4e)**. Examples of TM^{3+} are Sc, Ti, and Cr, and TM^{4+} are Zr, Hf, and Pt.[12] Pd brings additional modes of metal occupancy and metal-sulfur unit geometry. Structures with Pd^{2+} and a smaller tetrel (Si) exhibit edge-sharing distorted square planar [PdS_4] units (**Figure 4d**) which can be obtained from an octahedron by elongation of the axial Pd-S bond lengths. Switching to a bigger tetrel (Ge) resulted in the formation of strongly distorted [PdS_6] octahedra (**Figure 4c**). In this case, Pd is split between two positions: the center of the octahedra and near the center of the trigonal faces of the octahedra. Finally, combining Cu and Pd in the Si-containing structure, Pd^{2+} forms regular face-sharing [PdS_6] octahedral units with the Cu+ occupying the trigonal faces as [CuS_3] (**Figure 4b)**.

Synthesis. Bulk powder for $La_6PdSi_2S_{14}$ was prepared by combining the arc-melted La_6PdSi_2 precursor with sulfur in a 1 : 14 ratio in a sealed ampoule and dwelling the mixture at 1050 ^oC for 72 hours (**Figure 5**). The crystals for Pd-Si, Pd-Ge, and Pd/Cu-Si analogues were grown by combining the appropriate arc-melted precursors, sulfur, and potassium iodide (KI) flux in 1 : 30 mass ratio in a sealed ampoule and dwelling at 1000 ^oC for 72 hours. The mechanism of such reactions can be proposed based on the *in situ* data for $La_6Rh_{0.67}Si_2S_{14}$, where the metal tetrelide precursor decomposes via reaction with sulfur to form a highly reactive mixture of binary sulfides which further combine to form the multinary phases.[12]

Journal Pre-proof

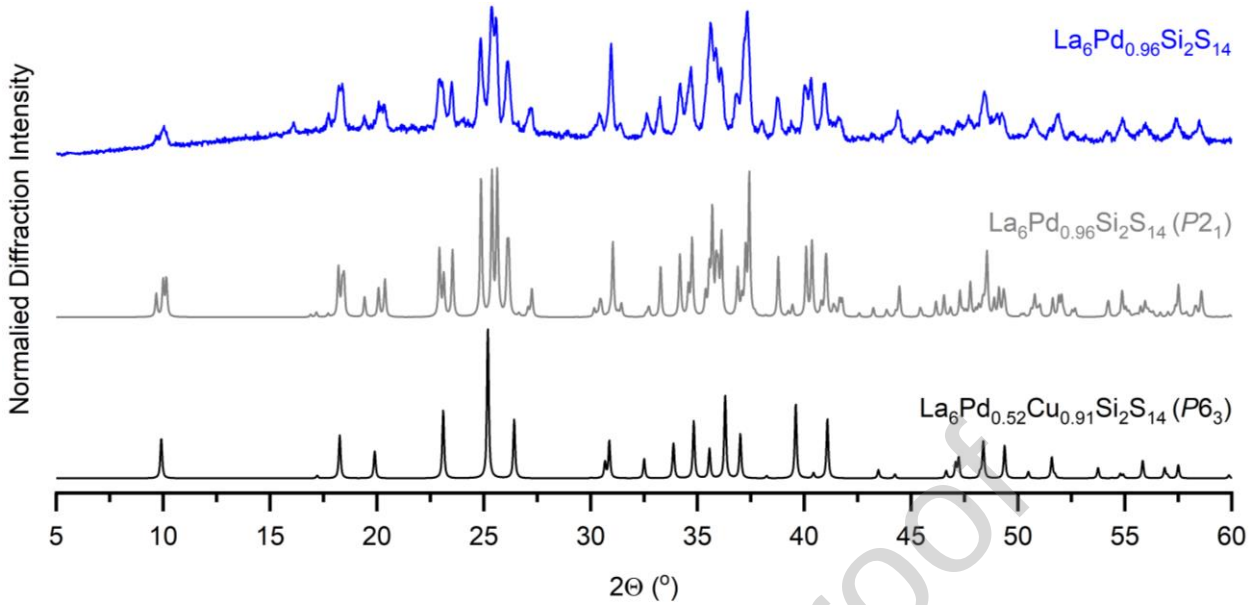

Figure 5. An experimental powder X-ray diffraction pattern for $La_6Pd_{0.96}Si_2S_{14}$ (blue). Patterns in black and gray are calculated from single crystal data for $La_6Pd_{0.96}Si_2S_{14}$ ($P2_1$) and $La_6Pd_{0.52}Cu_{0.91}Si_2S_{14}$ ($P6_3$).

SEM/EDS. To validate the phase composition and the transition metal content derived from single crystal structure determination, energy-dispersive spectroscopy (EDS) was used (**Table 1**). In all three cases, there is an agreement for the content of Pd and Cu in the samples.

ELECTRONIC STRUCTURE CALCULATIONS. Density functional theory (DFT) calculations were employed to study the electronic structure of $La_6PdSi_2S_{14}$. Two different structural models were constructed – monoclinic and hexagonal – to probe potential reasons for the observed monoclinic structural distortion. The monoclinic model was based on the $La_6PdSi_2S_{14}$ experimental crystal structure reported herein and features [PdS_4] square planar units, while the hexagonal model was based on the $La_6NiSi_2S_{14}$ structure-type and features [PdS_6] octahedra.

Journal Pre-proof

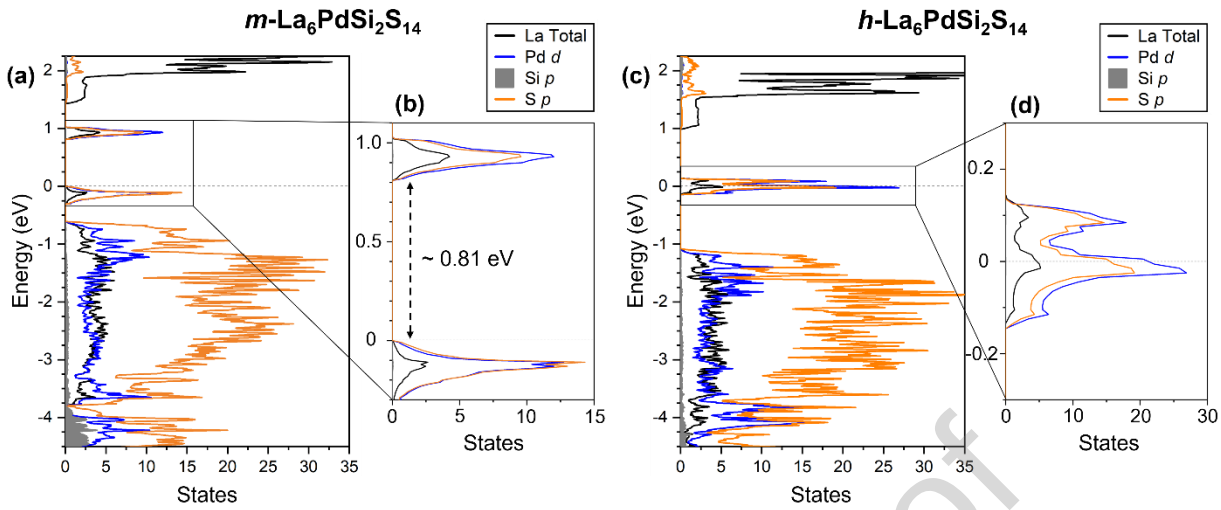

Figure 6. Density of states (DOS) curves for (a) monoclinic and (c) hypothetical hexagonal models of $La_6PdSi_2S_{14}$. (b, d) Orbital contributions nearest to Fermi level are shown for the monoclinic and hexagonal models, respectively. Partial DOS curves are shown for La total (black), Pd *d* (blue), Si *p* (grey filled), and S *p* (orange) states. The Fermi level is given by a dashed black line.

To account for the partial occupancy of the Pd^{2+} in the crystal structure models, 1×1×2 supercells were used. Pd atoms were placed in alternating square planar or octahedral units in the chains and, to simplify the calculations, split occupancy of S sites was ignored. The constructed models were relaxed and their total energies were compared. Compared to the hypothetical hexagonal structure, the monoclinic structure of $La_6PdSi_2S_{14}$ is lower in energy by ~19.6 meV/atom which corroborates experimental findings. The difference between these two structural models becomes more pronounced when comparing the density of states (DOS) of the two materials.

The DOS for both $La_6PdSi_2S_{14}$ models share fundamental features (**Figure 6**). The valence band has primarily S 3*p* character with substantial contributions from Pd 4*d* and La states and minor contribution from Si 3*p* states. The conduction band is dominated by La states with some hybridization of orbitals associated with Pd, Si, and S. The electronic structures of the monoclinic and hexagonal structural models are distinct at the region closest to the Fermi level. The hypothetical hexagonal model has a significant number of states at the Fermi level suggesting metallic character. These states originate from significant hybridization of S 3*p* and Pd 4*d* orbitals with minor contribution from La states. However, in the monoclinic

model, these states split to just below and above the Fermi level, which opens up a bandgap of 0.81 eV. While underestimated, the calculated bandgap agrees reasonably with the measured optical bandgap of 1.41 eV (**Figure 7 inset**). The splitting of Pd-S states in the monoclinic model is likely due to the Jahn-Teller distortion of pseudo-[PdS_6] units in the structure which eliminates band degeneracies near the Fermi level. In a word, the structural distortion of Pd-containing units in $La_6PdSi_2S_{14}$ gives rise to the semiconducting behavior of the phase and makes it a viable candidate for NLO materials.

Similar studies were conducted to further understand why this structural distortion is not observed with metals such as Ni^{2+}, which adopts an octahedral coordination environment. Qualitatively, the DOS of hexagonal and monoclinic models of $La_6NiSi_2S_{14}$ are similar to those of the Pd counterparts. In fact, the difference in energy between the two models for Ni-containing compounds still suggests the monoclinic model is preferred. However, the magnitude of this energy difference is smaller (~13 meV/atom). One potential cause for the discrepancy between computed and experimental findings is the exclusion of magnetic interactions of d^8 Ni^{2+}. Knowledge of the magnetic structure of $La_6NiSi_2S_{14}$ is needed to accurately conduct such calculations to observe if splitting of spin up/spin down channels results in any additional stabilization of one structural model over the other. Related studies are currently underway to probe magnetic structure of $RE_6TMSi_2S_{14}$ and its effect on structure-property relationships in this family of materials.

Optical Properties. $La_6PdSi_2S_{14}$ crystallizes in the non-centrosymmetric $P2_1$ space group and is a semiconductor with a 1.41 eV experimental band gap as determined by UV-vis spectroscopy. Therefore, it is a good candidate for infrared non-linear optical applications. **Table 6 and Figure 7** show the comparison of SHG and LDT data for $La_6PdSi_2S_{14}$, previously reported $La_6Cu_2Ge_2S_{14}$, and the state-of-the-art IR NLO standard $AgGaS_2$. Both these quaternary sulfides show good SHG activities which are at least twice that of the

standard and, furthermore, the data show phase-matchability for both materials. $La_6PdSi_2S_{14}$ shows a good combination of SHG and LDT (3× $AgGaS_2$) as compared to other recent reports for quaternary sulfides.[12,13,47] Both phases have transition metals in non-octahedral geometries – distorted-[PdS_4] and trigonal planar-[CuS_3] – which could be important for the good non-linear optical properties. SHG response is typically smaller in materials with larger band gaps, while LDT is large in wide band gap materials.[13,47] Interestingly, although the Pd and Cu analogues show similar SHG values, they have vastly different band gap values (1.41 vs 2.5 eV, respectively), which could indicate that other than bandgap factors contribute to the enhanced SHG properties. Furthermore, the distorted nature of the [PdS_4] units may contribute to the properties enhancement, similar to the distorted tetrahedral units in $Hg_3P_2S_8$ which were shown to be the key to the good non-linear optical properties.[14,15] Unfortunately, we were not able to produce single-phase samples of mixed Pd-Cu compound with a combination of triangular and square-planar units. Additional disorder can be introduced into the structure by combining Pd with *TM*'s which prefer to form [(*TM*)S_6] octahedra (e.g. *TM* = Ni or Pt) that may further distort the structure. However, attempts to synthesize such phases has proved to be a difficult task due to tendency for phase segregation into *TM*-rich $P6_3$ and Pd-rich $P2_1$ structures.

Journal Pre-proof

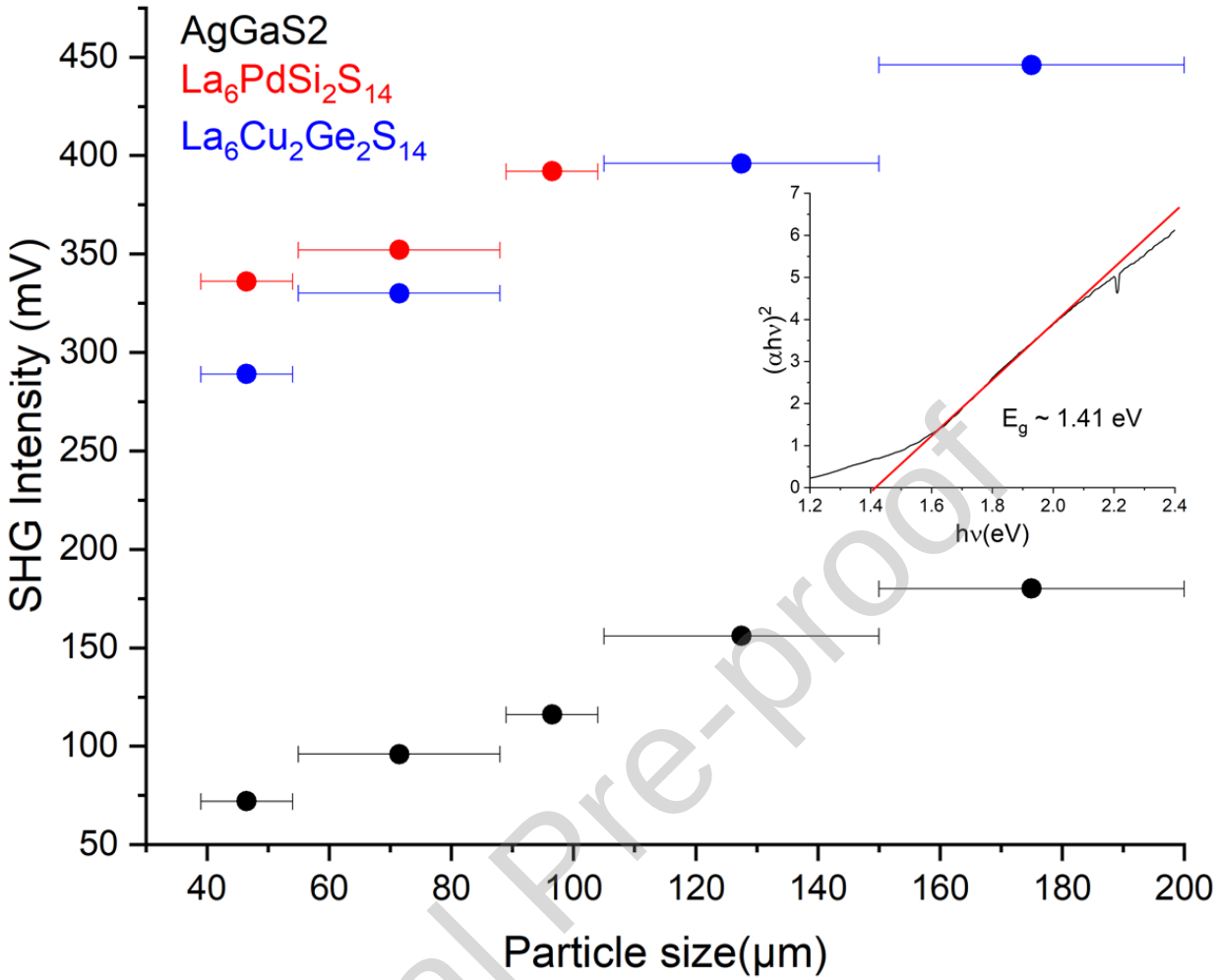

Figure 7. Second-harmonic generation (SHG) data for $La_6PdSi_2S_{14}$ (red), $La_6Cu_2Ge_2S_{14}$ (blue)[12], and $AgGaS_2$ standard (black). Inset: Optical band gap for $La_6PdSi_2S_{14}$ measured using diffuse reflectance.

Table 6. Summary of non-linear optical data for $La_6PdSi_2S_{14}$, $La_6Cu_2Ge_2S_{14}$, and $AgGaS_2$ standard.

Phase	[TMS_x] geometry	Band Gap (eV)	SHG (mV) (55-88 μm part. size)	SHG (×$AgGaS_2$)	LDT (MW/cm^2)	LDT (×$AgGaS_2$)
$AgGaS_2$	T_d	2.50	96	1.0	29.6	1.0
$La_6Pd_{0.96}Si_2S_{14}$	$\square_{plan}$	1.41	352	3.7	89.0	3.0
$La_6Cu_2Ge_2S_{14}$	Δ_{plan}	2.57	330	3.4	41.5	1.4

CONCLUSIONS

In this manuscript, we reported a unique member of the $(RE)_6(TM)_x(Tt)_2Q_{14}$ family of compounds, $La_6PdSi_2S_{14}$ which, unlike its group members, crystallizes in the non-centrosymmetric monoclinic $P2_1$ space group. The structure is characterized by Pd forming distorted square planar [PdS_4] units which share edges to form chains. We further report that it is possible to stabilize Pd-containing $(RE)_6(TM)_xSi_2S_{14}$ in the hexagonal $P6_3$ structure by

forming a solid solution with Cu, such as $La_6Pd_{0.5}CuSi_2S_{14}$, where Pd forms [PdS_6] octahedra and Cu forms trigonal-planar [CuS_3] units occupying the opposite faces of the octahedra. The highly disordered nature of [PdS_4] in the structure of $La_6PdSi_2S_{14}$ is responsible for the excellent NLO properties: SHG (3.7× $AgGaS_2$) and LDT (3× $AgGaS_2$) as well as phase matchability. This shows the promise of square-planar structural motifs for the enhancement of NLO properties for novel materials.

AUTHOR INFORMATION

CORRESPONDING AUTHOR

Prof. Kirill Kovnir, kovnir@iastate.edu

AUTHOR CONTRIBUTIONS

The manuscript was written through contributions of all authors. Authors declare no conflict of interests.

FUNDING SOURCES

G.A. is grateful to the Ames Laboratory Spedding Postdoctoral Fellowship for financial support. This work was supported by the Ames Laboratory's Laboratory Directed Research and Development (LDRD) program (G.A., G.V., N.W.H., K.K.). N.W.H. was supported by the U.S. Department of Energy Office of Science, Science Undergraduate Laboratory Internships (SULI). The Ames Laboratory is operated for the U.S. DOE by Iowa State University under contract #DE-AC02-07CH11358.

ACKNOWLEDGMENT

We thank Prof. V. Pecharsky (ISU and Ames Laboratory) for access to the arc-melting setup and Professor Javier Vela (ISU) for the use of the diffuse-reflectance setup.

ORCID

Journal Pre-proof

Georgiy Akopov 0000-0001-9399-9850
Gayatri Viswanathan 0000-0002-9693-8225
Nethmi Hewage 0000-0001-7062-7114
Philip Yox 0000-0002-8524-8202
Kui Wu 0000-0001-8242-4613
Kirill A. Kovnir 0000-0003-1152-1912

Journal Pre-proof

REFERENCES

(1) Nikogosyan, D. N. *Nonlinear Optical Crystals: A Complete Survey*; Springer-Science: New York, 2005.

(2) Boyd, R. W. *Nonlinear Optics*, 3rd ed.; Elsevier Science, 2008.

(3) Petrov, V. Progress in 1-Mm Pumped Mid-IR Optical Parametric Oscillators Based on Non-Oxide Nonlinear Crystals. *IEEE J. Select. Topics Quantum Electron.* **2015**, *21* (1), 193–206. https://doi.org/10.1109/JSTQE.2014.2378595.

(4) Petrov, V. Frequency Down-Conversion of Solid-State Laser Sources to the Mid-Infrared Spectral Range Using Non-Oxide Nonlinear Crystals. *Progress in Quantum Electronics* **2015**, *42*, 1–106. https://doi.org/10.1016/j.pquantelec.2015.04.001.

(5) Isaenko, L. I.; Yelisseyev, A. P. Recent Studies of Nonlinear Chalcogenide Crystals for the Mid-IR. *Semicond. Sci. Technol.* **2016**, *31* (12), 123001. https://doi.org/10.1088/0268-1242/31/12/123001.

(6) Mutailipu, M.; Poeppelmeier, K. R.; Pan, S. Borates: A Rich Source for Optical Materials. *Chem. Rev.* **2021**, *121* (3), 1130–1202. https://doi.org/10.1021/acs.chemrev.0c00796.

(7) Chen, J.; Lin, C.; Zhao, D.; Luo, M.; Peng, G.; Li, B.; Yang, S.; Sun, Y.; Ye, N. Anionic Aliovalent Substitution from Structure Models of ZnS: Novel Defect Diamond- like Halopnictide Infrared Nonlinear Optical Materials with Wide Band Gaps and Large SHG Effects. *Angew. Chem. Int. Ed.* **2020**, *59* (52), 23549–23553. https://doi.org/10.1002/anie.202010319.

(8) Li, G.; Wu, K.; Liu, Q.; Yang, Z.; Pan, S. $Na_2ZnGe_2S_6$: A New Infrared Nonlinear Optical Material with Good Balance between Large Second-Harmonic Generation Response and High Laser Damage Threshold. *J. Am. Chem. Soc.* **2016**, *138* (23), 7422–7428. https://doi.org/10.1021/jacs.6b03734.

(9) Li, S.-F.; Jiang, X.-M.; Fan, Y.-H.; Liu, B.-W.; Zeng, H.-Y.; Guo, G.-C. New Strategy for Designing Promising Mid-Infrared Nonlinear Optical Materials: Narrowing the Band Gap for Large Nonlinear Optical Efficiencies and Reducing the Thermal Effect for a High Laser-Induced Damage Threshold. *Chem. Sci.* **2018**, *9* (26), 5700–5708. https://doi.org/10.1039/C8SC01210E.

(10) Wu, K.; Chu, Y.; Yang, Z.; Pan, S. $A_2SrM^{IV}S_4$ (A = Li, Na; M^{IV} = Ge, Sn) Concurrently Exhibiting Wide Bandgaps and Good Nonlinear Optical Responses as New Potential Infrared Nonlinear Optical Materials. *Chem. Sci.* **2019**, *10* (14), 3963–3968. https://doi.org/10.1039/C9SC00028C.

(11) Ye, Z.; Bardelli, S.; Wu, K.; Sarkar, A.; Swindle, A.; Wang, J. Synthesis, Crystal Growth, Electronic Properties and Optical Properties of $Y_6IV_{2.5}S_{14}$ (IV = Si, Ge). *Z. anorg. allg. Chem.* **2021**, zaac.202100271. https://doi.org/10.1002/zaac.202100271.

(12) Akopov, G.; Hewage, N. W.; Yox, P.; Viswanathan, G.; Lee, S. J.; Hulsebosch, L. P.; Cady, S. D.; Paterson, A. L.; Perras, F. A.; Xu, W.; Wu, K.; Mudryk, Y.; Kovnir, K. Synthesis-Enabled Exploration of Chiral and Polar Multivalent Quaternary Sulfides. *Chem. Sci.* **2021**, *12*, 14718–14730. https://doi.org/10.1039/D1SC03685H.

(13) Yang, Y.; Chu, Y.; Zhang, B.; Wu, K.; Pan, S. Unique Unilateral-Chelated Mode-Induced d–P−π Interaction Enhances Second-Harmonic Generation Response in New Ln_3LiMS_7 Family. *Chem. Mater.* **2021**, *33* (11), 4225–4230. https://doi.org/10.1021/acs.chemmater.1c01133.

(14) Chu, Y.; Wang, P.; Zeng, H.; Cheng, S.; Su, X.; Yang, Z.; Li, J.; Pan, S. $Hg_3P_2S_8$: A New Promising Infrared Nonlinear Optical Material with a Large Second-Harmonic Generation and a High Laser-Induced Damage Threshold. *Chem. Mater.* **2021**, *33* (16), 6514–6521. https://doi.org/10.1021/acs.chemmater.1c01982.

(15) Xing, W.; Liang, F.; Tang, C.; Uykur, E.; Lin, Z.; Yao, J.; Yin, W.; Kang, B. Highly Distorted [HgS_4] Motif-Driven Structural Symmetry Degradation and Strengthened Second-Harmonic Generation Response in the Defect Diamond-Like Chalcogenide $Hg_3P_2S_8$. *ACS Appl. Mater. Interfaces* **2021**, *13* (31), 37331–37338. https://doi.org/10.1021/acsami.1c06933.
(16) Pielnhofer, F.; Schoop, L. M.; Kuhn, A.; Eger, R.; Nuss, J.; Nuss, H.; Lotsch, B. V. New Light on an Old Story: The Crystal Structure of Boron Tetrathiophosphate Revisited *Z. Anorg. Allg. Chem.* **2019**, *645* (3), 267–271. https://doi.org/10.1002/zaac.201800460.
(17) Chu, Y.; Li, G.; Su, X.; Wu, K.; Pan, S. A Review on the Development of Infrared Nonlinear Optical Materials with Triangular Anionic Groups. *Journal of Solid State Chemistry* **2019**, *271*, 266–272. https://doi.org/10.1016/j.jssc.2018.10.051.
(18) Luo, X.; Li, Z.; Guo, Y.; Yao, J.; Wu, Y. Recent Progress on New Infrared Nonlinear Optical Materials with Application Prospect. *Journal of Solid State Chemistry* **2019**, *270*, 674–687. https://doi.org/10.1016/j.jssc.2018.12.036.
(19) Akopov, G.; Viswanathan, G.; Kovnir, K. Synthesis, Crystal and Electronic Structure of La_2SiP_4. *Z. Anorg. Allg. Chem.* **2021**, *647* (2–3), 91–97. https://doi.org/10.1002/zaac.202000378.
(20) Akopov, G.; Mark, J.; Viswanathan, G.; Lee, S. J.; McBride, B. C.; Won, J.; Perras, F. A.; Paterson, A. L.; Yuan, B.; Sen, S.; Adeyemi, A. N.; Zhang, F.; Wang, C.-Z.; Ho, K.-M.; Miller, G. J.; Kovnir, K. Third Time's the Charm: Intricate Non-Centrosymmetric Polymorphism in *Ln*SiP_3 (*Ln* = La and Ce) Induced by Distortions of Phosphorus Square Layers. *Dalton Trans.* **2021**, *50* (19), 6463–6476. https://doi.org/10.1039/D1DT00845E.
(21) Lee, S. J.; Won, J.; Wang, L.; Jing, D.; Harmer, C. P.; Mark, J.; Akopov, G.; Kovnir, K. New Noncentrosymmetric Tetrel Pnictides Composed of Square- Planar Gold(I) with Peculiar Bonding. *Chem. Eur. J.* **2021**, *27* (26), 7383–7390. https://doi.org/10.1002/chem.202005312.
(22) Lee, S.; Carnahan, S. L.; Akopov, G.; Yox, P.; Wang, L.; Rossini, A. J.; Wu, K.; Kovnir, K. Noncentrosymmetric Tetrel Pnictides $RuSi_4P_4$ and $IrSi_3P_3$: Nonlinear Optical Materials with Outstanding Laser Damage Threshold. *Adv. Funct. Mater.* **2021**, *31* (16), 2010293. https://doi.org/10.1002/adfm.202010293.
(23) Sheldrick, G. M. A Short History of *SHELX*. *Acta Crystallogr A Found Crystallogr* **2008**, *64* (1), 112–122. https://doi.org/10.1107/S0108767307043930.
(24) Kresse, G.; Furthmüller, J. Efficient Iterative Schemes for *Ab Initio* Total-Energy Calculations Using a Plane-Wave Basis Set. *Phys. Rev. B* **1996**, *54* (16), 11169–11186. https://doi.org/10.1103/PhysRevB.54.11169.
(25) Kresse, G.; Joubert, D. From Ultrasoft Pseudopotentials to the Projector Augmented-Wave Method. *Phys. Rev. B* **1999**, *59* (3), 1758–1775. https://doi.org/10.1103/PhysRevB.59.1758.
(26) Blöchl, P. E. Projector Augmented-Wave Method. *Phys. Rev. B* **1994**, *50* (24), 17953–17979. https://doi.org/10.1103/PhysRevB.50.17953.
(27) Perdew, J. P. Density Functional Theory and the Band Gap Problem. *Int. J. Quantum Chem.* **1985**, *28* (S19), 497–523. https://doi.org/10.1002/qua.560280846.
(28) Perdew, J. P.; Burke, K.; Ernzerhof, M. Generalized Gradient Approximation Made Simple. *PHYSICAL REVIEW LETTERS* **1996**, *77* (18), 4.
(29) Blöchl, P. E.; Jepsen, O.; Andersen, O. K. Improved Tetrahedron Method for Brillouin-Zone Integrations. *Phys. Rev. B* **1994**, *49* (23), 16223–16233. https://doi.org/10.1103/PhysRevB.49.16223.
(30) Monkhorst, H. J.; Pack, J. D. Special Points for Brillouin-Zone Integrations. *Phys. Rev. B* **1976**, *13* (12), 5188–5192. https://doi.org/10.1103/PhysRevB.13.5188.

Journal Pre-proof

(31) Chen, J.; Lin, C.; Peng, G.; Xu, F.; Luo, M.; Yang, S.; Shi, S.; Sun, Y.; Yan, T.; Li, B.; Ye, N. $BaGe_2Pn_2$ (Pn = P, As): Two Congruent-Melting Non-Chalcopyrite Pnictides as Mid- and Far-Infrared Nonlinear Optical Materials Exhibiting Large Second Harmonic Generation Effects. *Chem. Mater.* **2019**, *31* (24), 10170–10177. https://doi.org/10.1021/acs.chemmater.9b03863.

(32) Sun, Y.; Chen, J.; Yang, S.; Li, B.; Chai, G.; Lin, C.; Luo, M.; Ye, N. $LaSiP_3$ and $LaSi_2P_6$: Two Excellent Rare- Earth Pnictides with Strong SHG Responses as Mid- and Far- Infrared Nonlinear Optical Crystals. *Adv. Optical Mater.* **2021**, 2002176. https://doi.org/10.1002/adom.202002176.

(33) Michelet, A.; Flahaut, M. J. Sur les composes du type $La_6MnSi_2S_{14}$. *C. R. Acad. Sc. Paris - Serie C* **1969**, *269*, 1203–1205.

(34) Iyer, A. K.; Yin, W.; Lee, E. J.; Lin, X.; Mar, A. Quaternary Rare-Earth Sulfides $RE_3M_{0.5}GeS_7$ (RE=La–Nd, Sm; M=Co, Ni) and $Y_3Pd_{0.5}SiS_7$. *Journal of Solid State Chemistry* **2017**, *250*, 14–23. https://doi.org/10.1016/j.jssc.2017.03.009.

(35) Daszkiewicz, M.; Gulay, L. D.; Lychmanyuk, O. S.; Pietraszko, A. Crystal Structure of the $R_3Ag_{1-\delta}SiS_7$ (R=La, Ce, Pr, Nd, Sm, Δ=0.10–0.23) Compounds. *Journal of Alloys and Compounds* **2008**, *460* (1–2), 201–205. https://doi.org/10.1016/j.jallcom.2007.05.067.

(36) Brese, N. E.; Squattrito, P. J.; Ibers, J. A. Reinvestigation of the Structure of PdS. *Acta Crystallogr C Cryst Struct Commun* **1985**, *41* (12), 1829–1830. https://doi.org/10.1107/S0108270185009623.

(37) Knop, O.; Huang, C.-H.; Reid, K. I. G.; Carlow, J. S. Chalkogenides of the Transition Elements. X. X-Ray, Neutron, Mossbauer and Magnetic Studies of Pentlandite and the π Phases π(Fe,Co,Ni,S), Co_8MS_8, and $Fe_4Ni_4MS_8$ (M = Ru, Rh, Pd). *Journal of Solid State Chemistry* **1976**, *16*, 97–116.

(38) Huster, J.; Bronger, W. Synthesis and Structure of $BaPdS_2$. *Journal of the Less Common Metals* **1986**, *119* (1), 159–165. https://doi.org/10.1016/0022-5088(86)90206-7.

(39) Bronger, W.; Huster, J. Cs2Pd3S4, Ein Neuer Schichtenstrukturtyp. *Journal of the Less Common Metals* **1971**, *23*, 67–73.

(40) Klingen, W.; Ott, R.; Hahn, H. Uber die Darstellung und Eigenschaften von Hexathio- und Hexaselenohypodiphosphaten. *Z. Anorg. Allg. Chem.* **1973**, *396* (3), 271–278. https://doi.org/10.1002/zaac.19733960305.

(41) Bronger, W.; Gunther, O.; Huster, J.; Spangenberg, M. Uber Die Kettenstruktur Der Verbindungen Na_2PdS_2 Und Pa2PtS2. *Journal of the Less Common Metals* **1976**, *50*, 49–55.

(42) Keszler, D. A.; Ibers, J. A.; Mueller, M. H. Preparation, Characterization, and Physical Properties of the Series MPd_3S_4 (M = Rare Earth). *J. Chem. Soc., Dalton Trans.* **1985**, No. 11, 2369. https://doi.org/10.1039/dt9850002369.

(43) Zhang, X.; Luo, Z.; Yu, P.; Cai, Y.; Du, Y.; Wu, D.; Gao, S.; Tan, C.; Li, Z.; Ren, M.; Osipowicz, T.; Chen, S.; Jiang, Z.; Li, J.; Huang, Y.; Yang, J.; Chen, Y.; Ang, C. Y.; Zhao, Y.; Wang, P.; Song, L.; Wu, X.; Liu, Z.; Borgna, A.; Zhang, H. Lithiation-Induced Amorphization of $Pd_3P_2S_8$ for Highly Efficient Hydrogen Evolution. *Nat Catal* **2018**, *1* (6), 460–468. https://doi.org/10.1038/s41929-018-0072-y.

(44) Daoudi, A.; Noel, H. Sulfures Ternaires D'Uranium et de Palladium: III. Caracterisation et Structure Cristalline de PdU_2S_4. *Journal of the Less Common Metals* **1986**, *115*, 253–259.

(45) Keszler, D. A.; Squattrito, P. J.; Brese, N. E.; Ibers, J. A.; Shang, M.; Lu, J. New Layered Ternary Chalcogenides: Tantalum Palladium Sulfide (Ta_2PdS_6), Tantalum Palladium Selenide (Ta_2PdSe_6), Niobium Palladium Sulfide (Nb_2PdS_6), Niobium

Palladium Selenide (Nb_2PdSe_6). *Inorg. Chem.* **1985**, *24* (19), 3063–3067. https://doi.org/10.1021/ic00213a038.

(46) Chondroudis, K.; Kanatzidis, M. G.; Sayettat, J.; Jobic, S.; Brec, R. Palladium Chemistry in Molten Alkali Metal Polychalcophosphate Fluxes. Synthesis and Characterization of $K_4Pd(PS_4)_2$, $Cs_4Pd(PSe_4)_2$, $Cs_{10}Pd(PSe_4)_4$, $KPdPS_4$, $K_2PdP_2S_6$, and $Cs_2PdP_2Se_6$. *Inorg. Chem.* **1997**, *36* (25), 5859–5868. https://doi.org/10.1021/ic970593n.

(47) Shi, Y.-F.; Chen, Y.; Chen, M.-C.; Wu, L.-M.; Lin, H.; Zhou, L.-J.; Chen, L. Strongest Second Harmonic Generation in the Polar R_3MTQ_7 Family: Atomic Distribution Induced Nonlinear Optical Cooperation. *Chem. Mater.* **2015**, *27* (5), 1876–1884. https://doi.org/10.1021/acs.chemmater.5b00177.

Journal Pre-proof

Graphical abstract

TOC Figure

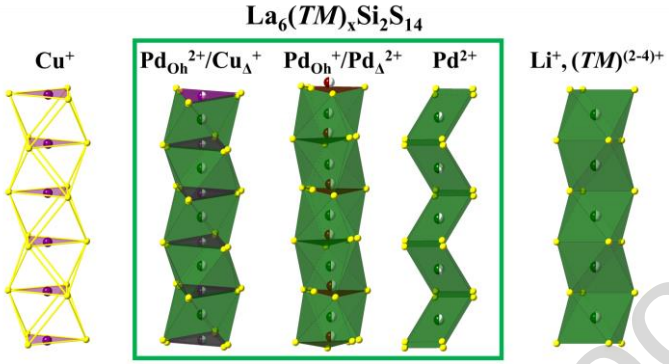

Journal Pre-proof

CRediT author statement

***Georgiy Akopov, Gayatri Viswanathan, Nethmi W. Hewage, Philip Yox, Kui Wu, Kirill Kovnir*:** Investigation ***Georgiy Akopov, Kirill Kovnir**:* Supervision. **All authors:** Writing-Reviewing and Editing.

Declaration of interests

☒The authors declare that they have no known competing financial interests or personal relationships that could have appeared to influence the work reported in this paper.

☐The authors declare the following financial interests/personal relationships which may be considered as potential competing interests:

Journal Pre-proof

Highlights

- Novel member of $La_6(TM)Si_2S_{14}$ family is reported with *TM* = Pd.
- Local coordination of Pd is square planar unlike octahedral for *TM* = Ni and Pt.
- Pd crystal structure distorts from hexagonal to monoclinic symmetry.
- $La_6PdSi_2S_{14}$ exhibits remarkable NLO properties with high SHG and LDT.

Journal Pre-proof